Hexamethylcyclopentadiene: time-resolved photoelectron spectroscopy and *ab initio* multiple spawning simulations†

T. J. A. Wolf,*[ab] T. S. Kuhlman,[c] O. Schalk,[de] T. J. Martínez,[bf] K. B. Møller,[c] A. Stolow[egh] and A.-N. Unterreiner*[a]

Progress in our understanding of ultrafast light-induced processes in molecules is best achieved through a close combination of experimental and theoretical approaches. Direct comparison is obtained if theory is able to directly reproduce experimental observables. Here, we present a joint approach comparing time-resolved photoelectron spectroscopy (TRPES) with *ab initio* multiple spawning (AIMS) simulations on the MS-MR-CASPT2 level of theory. We disentangle the relationship between two phenomena that dominate the immediate molecular response upon light absorption: a spectrally dependent delay of the photoelectron signal and an induction time prior to excited state depopulation in dynamics simulations. As a benchmark molecule, we have chosen hexamethylcyclopentadiene, which shows an unprecedentedly large spectral delay of (310 ± 20) fs in TRPES experiments. For the dynamics simulations, methyl groups were replaced by "hydrogen atoms" having mass 15 and TRPES spectra were calculated. These showed an induction time of (108 ± 10) fs which could directly be assigned to progress along a torsional mode leading to the intersection seam with the molecular ground state. In a stepladder-type approach, the close connection between the two phenomena could be elucidated, allowing for a comparison with other polyenes and supporting the general validity of this finding for their excited state dynamics. Thus, the combination of TRPES and AIMS proves to be a powerful tool for a thorough understanding of ultrafast excited state dynamics in polyenes.

1 Introduction

Small polyenes are known to undergo ultrafast dynamics following the absorption of light. They can be regarded as model systems for the investigation of photoinduced processes in considerably larger biochemical structures because their dynamics are often restricted to a few relevant degrees of freedom. Interpretation of experimental data is, thus, much easier in these molecules. Furthermore, due to their relatively

few atoms, polyenes are amenable to high-level quantum mechanical simulations of their excited state dynamics. This is especially important because a profound understanding of photoinduced dynamics almost always necessitates a detailed comparison of experiment with theory. Many model systems have been investigated by time-resolved experiments[1–19] or dynamical simulations.[20–26] We believe that fundamental questions could be answered more easily by joint studies connecting experimental approaches with such simulations. However, very few studies of this type have been carried out so far.[27–31]

The direct comparison of experimental with simulated results is greatly facilitated when both yield the same observable for comparison. Time-resolved photoelectron spectroscopy (TRPES) meets the requirement for this since time-resolved photoelectron spectra can be synthesized *via* high-level dynamics simulations.[23,29,31] Furthermore, TRPES is sensitive to both the electronic character of a populated state and the vibrational dynamics, including large amplitude motions within that state,[32] allowing a detailed tracking of the coupled electronic–vibrational dynamics.

The present study aims at directly connecting two effects which have been observed in several studies of small polyenes.

[a] *Institut für Physikalische Chemie and Center for Functional Nanostructures (CFN), Karlsruhe Institute of Technology (KIT), Fritz-Haber-Weg 2, 76131 Karlsruhe, Germany. E-mail: andreas.unterreiner@kit.edu*

[b] *Stanford PULSE Institute, Menlo Park, California 94025, USA. E-mail: thomas.wolf@stanford.edu*

[c] *Department of Chemistry, Technical University of Denmark, Kemitorvet 207, DK-2800 Kgs. Lyngby, Denmark*

[d] *Stockholm University, AlbaNova University Center, SE-10691, Stockholm, Sweden*

[e] *National Research Council, 100 Sussex Drive, Ottawa, Canada*

[f] *Department of Chemistry, Stanford University, Stanford, California 94305, USA*

[g] *Department of Chemistry, University of Ottawa, Canada*

[h] *Department of Physics, University of Ottawa, Canada*

† Electronic supplementary information (ESI) available. See DOI: 10.1039/c4cp00977k

11770 | *Phys. Chem. Chem. Phys.*, 2014, **16**, 11770–11779

This journal is © the Owner Societies 2014

In time-resolved photoelectron spectra of these systems the earliest photoelectron band at time zero often does not appear at a constant delay time, but rather shows a time shift throughout the spectrum. This effect was attributed to large amplitude motion and to localization of the dynamics to a dynamophore, a dynamical subunit of the molecule, such as a single carbon double bond.[11,12,16,17,33]

Many dynamical simulations of small polyenes, on the other hand, show that population transfer from the initially excited to a lower lying electronic state is preceded by a time period during which the nuclear wavepacket needs to evolve along specific degrees of freedom in order to reach the conical intersection (CoIn) seam.[20,23] This period was referred to as an "induction time".[23,34,35]

In order to find a possible connection between the spectrally dependent time-delays in time-resolved photoelectron spectra and the induction time in dynamics simulations a benchmark system is needed in which both effects are readily apparent. For this, we require a system which exhibits a shift in time zero considerably larger than the experimental time resolution. Furthermore, the system has to be small enough that dynamics simulations remain feasible.

The cyclopentadiene (CPD) derivative hexamethylcyclopentadiene (CPDMe$_6$) meets both of these demands. CPD was previously investigated by TRPES and time-resolved mass spectroscopy.[5,8–10] The photoinduced dynamics were observed to be complete within less than 200 fs after photoexcitation. No shift in time zero was observed and the data were analyzed assuming a relaxation scheme which included three diabatic electronic states: the photoexcited state, a dark state, and the ground state. This was motivated by similar relaxation mechanisms observed in similar polyenic systems.[6,36–38] Furthermore, earlier calculations on the excited states of CPD[39] seemed to support this interpretation.

In a dynamical simulation of CPD,[40] however, only the first excited adiabatic state and the ground state were observed to be populated during the photoinduced dynamics.[23] The ground state population rise was observed to be delayed by an induction time of 31 fs. This finding suggests a slightly different mechanistic picture involving only two adiabatic states. Time-resolved photoelectron spectra were synthesized and seemed to agree with the experimental spectra. Yet, no quantitative comparison was performed.

The disagreement between the interpretations of these experimental and theoretical data may hint of a very small shift of time zero in the time-resolved photoelectron spectra which could not be resolved properly. In other words, the dynamics in CPD are too fast to serve as a test case for this connection between the time zero shift and the induction time. However, it was observed in TRPES studies of several systems, including CPD, that the excited state dynamics can be slowed by increasing substituent masses.[6,10,17,33,41] Hence, the dynamics would be expected to be considerably slower in the case of complete methyl substitution, as in hexamethylcyclopentadiene, CPDMe$_6$.

On the theoretical side, substitution of hydrogens by methyl groups is not desirable since it leads to a significant increase in computational demand. It has been, on the other hand, already shown that dynamical deceleration can be modelled in CPD by approximating the methyl groups as hydrogens with a mass of 15 amu.[23]

In the following, CPDMe$_6$ is studied by TRPES and by *ab initio* multiple spawning (AIMS) simulations on the MS-MR-CASPT2 level of theory, with the approximation of methyl groups as hydrogens of mass 15. To directly compare experimental with simulated data, time-resolved photoelectron spectra are synthesized from the dynamical simulations. As a check, agreement with earlier results is established by comparing to TRPES data of a different CPD derivative, 1,2,3,4-tetramethyl-5-propyl-cyclopentadiene (CPDMe$_4$PrH). Finally, experimental and theoretical time-resolved photoelectron spectra are compared by analyzing them *via* a stepladder-type model.

2 Methods

2.1 Experimental methods

CPDMe$_6$ was synthesized from 1,2,3,4,5-pentamethylcyclopentadiene (CPDMe$_5$H) *via* methylation according to the procedure described in the ESI.† Its purity is estimated to be >90%. 1,2,3,4-Tetramethyl-5-propyl-cyclopentadiene (CPDMe$_4$PrH) was purchased from Sigma Aldrich and used without further purification. Absorption spectra were recorded using a Varian Cary 500 and a Varian Cary 5e spectrometer.

For time-resolved experiments in the gas phase, a photoelectron spectrometer was employed, consisting of an amplified femtosecond Ti:Sa laser system and a magnetic bottle time of flight spectrometer in combination with a supersonic molecular beam. The setup is described in detail elsewhere.[42] Briefly, pump pulses at λ_p = 267 nm (2.5 μJ per pulse) were obtained by third harmonic generation from the output of the femtosecond laser system. Probe pulses at λ_{pr} = 320 nm (2 μJ per pulse) were generated by frequency quadrupling the output of an optical parametric amplifier. The relative polarization of pump and probe pulses was set to the magic angle. The pulses were collinearly focused into the interaction chamber of the magnetic bottle photoelectron spectrometer. The cross correlation of pump and probe pulses was measured using 1,4-diazabicyclo[2.2.2]octane and determined to be 130 ± 10 fs. In the interaction chamber, a supersonic molecular beam generated by a 1 kHz Even–Lavie valve with a 200 μm diameter conical nozzle intersected the optical beam path at the extraction region of the magnetic bottle. Helium was used as a carrier gas with a backing pressure of 3.4 bar. CPDMe$_6$ and CPDMe$_4$PrH were each introduced into the body of the valve as a liquid, soaked in a filter paper. Photoelectron kinetic energies were calibrated by using the known photoelectron spectrum of NO.[43]

2.2 Theoretical methods

2.2.1 Electronic structure, geometry optimizations and dynamical simulations. The details of electronic structure calculations, geometry optimizations and dynamical simulations are elaborated in ref. 23. Briefly, electronic structure

This journal is © the Owner Societies 2014

Phys. Chem. Chem. Phys., 2014, **16**, 11770–11779 | **11771**

calculations and geometry optimizations were carried out on the multi-state multi-reference complete active space second-order perturbation theory (MS-MR-CASPT2) level[44–46] employing the MOLPRO 2006.1 program package[47] and a 6-31G** basis set. No symmetry restriction was applied and levels were shifted by 0.2 Hartrees. The active space of the neutral species was chosen to consist of four electrons distributed over the two π and the two lowest lying $\pi^\star$ orbitals. It was, furthermore, averaged over the three lowest singlet states (SA-3-CAS(4,4)). Stationary points were optimized using routines included in MOLPRO, points of degeneracy between potential energy surfaces were optimized using either the CIOpt code[48] or a locally modified version of MOLPRO.

For the dynamical simulations, the in-house code was employed combining *ab initio* multiple spawning (AIMS) dynamics with electronic structure calculations performed in MOLPRO 2006.1[49] at the MS-MR-CASPT2/6-31G** level of theory with state-averaging over three states including analytic MS-MR-CASPT2 non-adiabatic coupling matrix elements.[25,50] The initial positions and momenta of trajectory basis functions (TBFs) were sampled from the same 0 K Wigner distribution as in ref. 23. The initial 38 TBFs were placed on S_1 and propagated for 290.3 fs (12 000 au) with a time step of 0.39 fs (16 au) using the independent first-generation approximation.[49,51] The final time was chosen long enough to capture the essential dynamics on the excited states. In cases where all population ($>99\%$) had been transferred to the ground state before the final time was reached, the calculation was stopped.

2.2.2 Simulation of TRPES. The methods employed for simulating time-resolved photoelectron spectra are detailed in ref. 23. Spectra were calculated considering the three neutral states from the dynamics calculations and two cationic states: the latter were calculated at the MS-MR-CAS(3,4)-PT2 level of theory with MOs taken from the CASSCF calculation of the neutral states. Dyson orbitals were calculated from the neutral and cationic MS-MR-CASPT2 mixing coefficients and CI vectors according to ref. 25. The transition matrix element was evaluated by using the ezDyson code.[52] The latter calculations employed a grid of $192 \times 192 \times 192$ points with a size of $12 \times 12 \times 12$ au^3, a maximum angular momentum $f = 7$, analytical isotropic averaging, and a Coulomb radial function for the free electron.

Systematic errors in the simulated time-resolved photoelectron spectra were corrected for by shifting the photoelectron kinetic energies by a factor

$$\Delta = \left[\delta E^{\text{exp,vert}}_{\text{S}_1 \leftarrow \text{S}_0} - \delta E^{\text{CASPT2}}_{\text{S}_1 \leftarrow \text{S}_0}(\text{Q}_{\text{FC}}) \right] \\ + \left[\text{IP}^{\text{CASPT2}}_{\text{D}_0 \leftarrow \text{S}_0}(\text{Q}_{\text{FC}}) - \text{IP}^{\text{exp,vert}}_{\text{D}_0 \leftarrow \text{S}_0} \right], \quad (1)$$

whereas δE indicates an energy difference between two neutral states, IP denotes the energy difference between the neutral ground state and the cationic ground state and Q_{FC} the Franck–Condon geometry. This procedure leads to a match between experimental and simulated photoelectron kinetic energies at least at time zero. For evaluation of Δ, the experimental IP of CPDMe$_5$H (7.35 eV) was employed, which is justified by

calculations of the IPs of CPDMe$_5$H (7.40 eV) and CPDMe$_6$ (7.40 eV) employing the outer-valence Green's function (OVGF) method as implemented in Gaussian 09[53] in combination with a QZVP basis.[54] Furthermore, it is assumed that the vertical excitation energy corresponds to the spectral position of the band maximum, *i.e.*, $\delta E^{\text{exp,vert}}_{\text{S}_1 \leftarrow \text{S}_0} = 4.84$ eV.

For the case of ionization by two probe photons ([1,2′]), the ionization probability could not be evaluated by the employed method. The probability was, therefore, set to unity. Thus, the relative intensities of [1,1′] and [1,2′] ionization spectra are not determined by the simulation.

For the simulated spectra, a Gaussian cross-correlation function of the pump and probe pulses with a full-width-at-half-maximum (FWHM) of 160 fs ([1,1′] ionization) and 139 fs ([1,2′] ionization) was assumed. The spectral resolution in the experiment was ≈ 25 meV due to the spectral bandwidth of the fs laser pulses. In contrast, a detection resolution of 150 meV was used in the simulation due to limited sampling.

3 Results

3.1 Absorption spectra and excited potential energy surfaces

The absorption spectra of CPD and CPDMe$_6$ in hexane are shown in Fig. 1. In both cases, only one absorption maximum can be found above $\lambda = 200$ nm. It can be unambiguously assigned to excitation into the lowest excited adiabatic state (S_1) characterized by a single electron LUMO $\leftarrow$ HOMO excitation and B_2 symmetry in the Franck–Condon (FC) region.

The substitution pattern of CPDMe$_6$ does not lead to a qualitative change in the spectrum, but rather to a red-shift of the absorption maximum from 241 nm to 256 nm and, thus, to a reduction of the S_1–S_0 gap as compared to CPD.

A visualization of the optimized minimum energy conical intersection (MECI) geometry of CPDMe$_6$ is included in Fig. 1(b). It is superimposed by one of the MECIs of CPD from ref. 23,
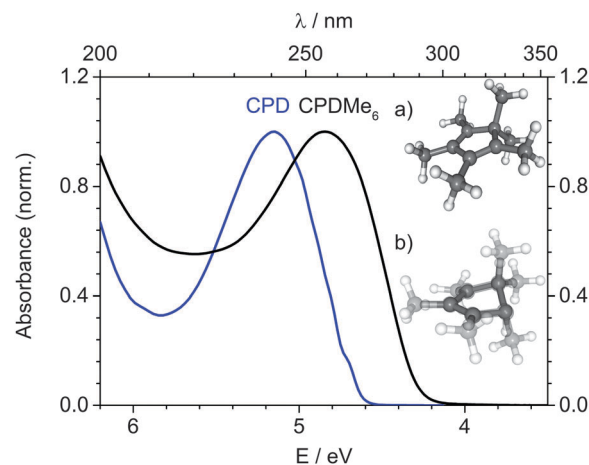

Fig. 1 Absorption spectrum of CPDMe$_6$ in hexane (black). For comparison the spectrum of CPD (blue) is shown. Inset are (a) the Franck–Condon structure of CPDMe$_6$ and (b) its MECI structure superimposed by a corresponding MECI structure of CPD as taken from ref. 23.

11772 | *Phys. Chem. Chem. Phys.*, 2014, **16**, 11770–11779

This journal is © the Owner Societies 2014

which was labeled there as "eth2-MECI". The superimposition shows very good agreement between the two MECI geometries. They can be identified as "ethylene-like" CoIns, since they primarily differ from the Franck–Condon (FC) geometries (see Fig. 1(a)) by torsion about one of the double bonds. Similar to the case of CPD, the diabatic character of S_1 experiences strong mixing with a higher diabatic state between the FC region and the CoIn region.[23]

Thus, methyl substitution does not seem to significantly alter the qualitative shape of the S_1 PES with respect to the degrees of freedom of the ring carbons. Hence, the approximation of methyl groups as hydrogens with mass 15 in the AIMS simulations is expected to yield results in high qualitative agreement with the experimental data. However, it introduces a quantitative change in the relative S_1 energy, which cannot be fully reproduced by the employed quantum chemical method (see the ESI† for details). Thus, there may be deviations in the overall time scales of the excited state dynamics due to a misestimation of the PES slope from the FC region to the CoIn.

3.2 Experimental TRPES

The time-resolved photoelectron spectra of $CPDMe_6$ resulting from excitation at λ_p = 267 nm (4.65 eV) and ionization at λ_{pr} = 320 nm (3.88 eV) are shown in Fig. 2(a). In the range between 0.2 and 1.3 eV, they exhibit an intense photoelectron band. In the range between 1.7 and 5.2 eV, only low photoelectron signals are found. In Fig. 2(a), the latter are magnified by a factor of 24. Both photoelectron bands exhibit a lifetime below 1 ps.

The IP of $CPDMe_6$ is estimated to be 7.35 eV (see Section 2.2.2). Accordingly, ionization of $CPDMe_6$ in the TRPES experiments can take place via one pump and one probe photon ([1,1']). In this [1,1'] ionization scheme, the maximum kinetic energy of the emitted photoelectron (at the temporal overlap of pump and probe pulses) is 1.18 eV. During the excited state dynamics, the initial wavepacket energy is increasingly transformed into nuclear kinetic energy leading to an increase in the

vertical IP as a function of time. As a consequence, kinetic energy of the emitted photoelectrons is reduced as a function of time. Hence, time-delayed photoelectron bands from [1,1'] ionization are expected to appear at kinetic energies between 0 and 1.18 eV. This expectation is seen in the intense photoelectron band between 0.2 and 1.3 eV in the time-resolved photoelectron spectra.

Conservation of energy dictates that the low intensity bands at kinetic energies above 1.3 eV can only originate from an ionization process involving more than one probe photon. The maximum photoelectron kinetic energy of a [1,2'] ionization is 5.06 eV and, thus, is consistent with the highest photoelectron kinetic energies observed in this band at around 5.2 eV. Hence, the time-resolved photoelectron spectra can be divided into a [1,1'] and a [1,2'] ionization regime, as indicated by the yellow line in Fig. 2(a). Accordingly, the underlying excited state dynamics leading to these two photoelectron bands are the same. Since the range of observable large amplitude photoelectron kinetic energies in the [1,2'] regime is larger than in the [1,1'] regime, the energetic observation window for the dynamics is larger in the case of [1,2'] ionization.

In each ionization regime, a broad photoelectron band can be seen. It is unstructured in the [1,1'] regime. The structures in the [1,2'] regime most likely stem from 2-photon ionization via resonant Rydberg states, as observed previously.[9] In both regimes, the photoelectron bands appear delayed and broadened in time towards lower photoelectron kinetic energies. Such a delay was earlier quantified by optimizing time-zero (t_0) as an additional parameter in a global 2D fitting routine of the experimental photoelectron spectra.[12,17,55] This was found to give a good measure of the overall shift. The t_0 values from a fit of the spectrum to delayed single-exponential fits are inserted as black circles in Fig. 2. Their maximum difference is (310 ± 20) fs, whereas the fitted time constant of the exponential decay is (180 ± 20) fs.
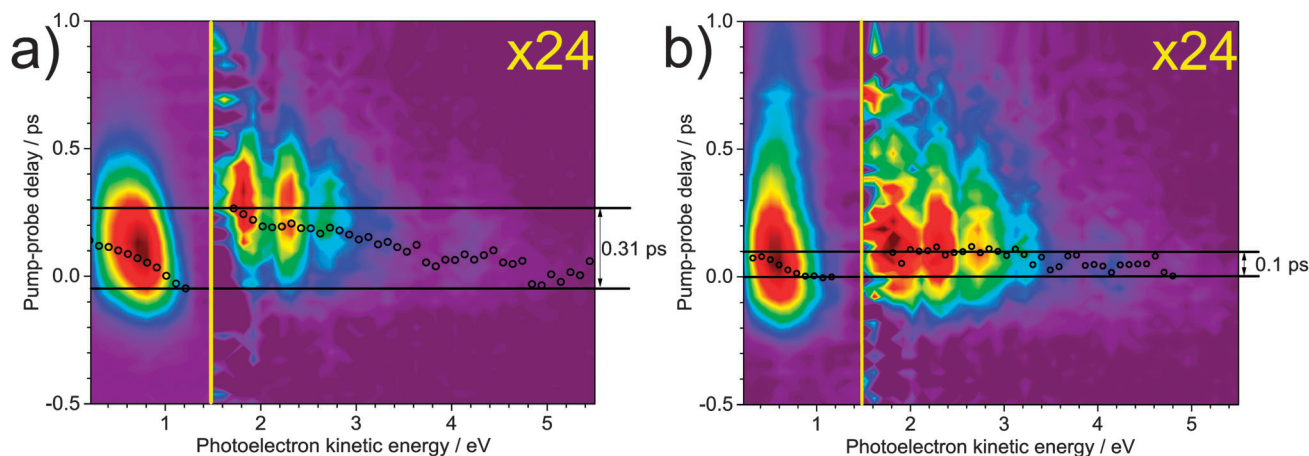
Fig. 2 Time-resolved photoelectron spectra of (a) $CPDMe_6$ and (b) $CPDMe_4PrH$ excited at λ_p = 267 nm and probed at λ_{pr} = 320 nm. The red color refers to high, the violet color to low photoelectron signals. Two regimes with high (left of yellow line) and low (right of yellow line) photoelectron intensities can be identified and associated with [1,1'] and [1,2'] ionization processes. The intensities in the [1,2'] regime are magnified by a factor of 24. The time-delay of the photoelectron bands, i.e. time-zero (t_0) values from an exponential fit with variable t_0, are inserted as black circles.

For comparison with the data published in ref. 10, we measured also time-resolved photoelectron spectra of CPDMe$_4$PrH. They are shown in Fig. 2(b) and can be rationalized analogously to the data from CPDMe$_6$ (for the absorption spectrum of CPDMe$_4$PrH see the ESI†). In addition to the photoelectron bands which were reported earlier, a weak band of longer life time is found in the [1,1′] regime. Its spectral signature overlaps with the signature of the strong, short-lived band. This new observation is most likely due to improved signal-to-noise ratios in the current experiment. The spectra also show a substantially smaller time-delay of (98 ± 4) fs, according to a biexponential fit with variable time zero. The global fits yield exponential time constants of (100 ± 30) fs and (500 ± 100) fs.

The apparent time delay of a photoelectron band was previously ascribed to both population transfer to a lower electronic state[56] and to vibrational redistribution within the initially populated excited state, *via* large-amplitude motions.[12,17] These two processes cannot be fully discerned *via* time-resolved, energy-resolved photoelectron spectra alone. We note, however, that angle-resolved photoelectron spectra, particularly in the molecular frame, may be able to differentiate these dynamics.[57]

3.3 Simulation of excited state dynamics of CPDMe$_6$

The AIMS simulations of CPDMe$_6$ give results similar to the earlier simulations on CPD. The only important channel for depopulating the initially excited S$_1$ state directly leads back to the ground state (see the time-dependence of S$_1$ population density in Fig. 3 and a plot including the S$_0$ and S$_2$ population densities in the ESI†). As in the case of CPD, the time evolution of S$_1$ population can be characterized by two parameters. Initially after preparation in the FC region of S$_1$, the wavepacket evolves for an induction period t_1 of (108 ± 1) fs in S$_1$, without observable electronic population loss. After the 108 fs delay, population transfer to S$_0$ begins. This population transfer is well described by a single exponential with a time constant t_2 = (54 ± 1) fs (see the ESI†). The values of the two time parameters indicate that, in comparison to the range of t_0 values from the global fits to the experimental time-resolved photoelectron spectra (see Fig. 2), the overall time scale of the dynamics is underestimated by the simulation.

The origin of the induction period is in time required for the molecule to redistribute potential energy into the distinct nuclear degrees of freedom which are important for accessing the conical intersection seam. Taking into account the "ethylene-like" character of the optimized MECI geometry (see Section 3.1), an obvious guess for such a degree of freedom is a torsion around one of the two double bonds (see inset of Fig. 3), achieving the highly twisted structure of one of the methyl substituents at the MECI geometry (see Fig. 1(b)). A projection of the time evolution of the S$_1$ wavepacket density onto this degree of freedom, together with the evolution of the overall S$_1$ population density shows a distinct correlation between the onset of population loss and the expectation value of the torsion coordinate changing from 9° to 30° (see Fig. 3). Projections of the S$_1$ wavepacket on other degrees of freedom, which also experience a major change between the
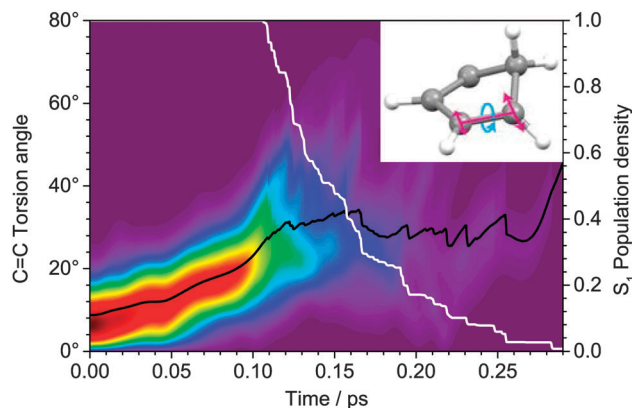

Fig. 3 Projection of the time evolution of the S$_1$ wavepacket density onto a torsional degree of freedom, as visualized in the inset. Red corresponds to high density, violet to low density. The time-dependent expectation value of the twisting angle is inserted as a black curve. Due to C_{2v} symmetry of the nuclear wavepacket, absolute torsion angles are employed. For comparison, the time-dependent S$_1$ population density is also inserted as a white curve. The onset of population density reduction nicely coincides with the torsion angle obtaining an expectation value of 30°.

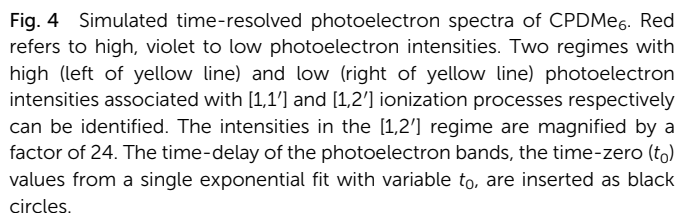FC and MECI geometries, do not show such a correlation (see the ESI†).

Due to C_{2v} symmetry of the molecule in the ground state, the S$_1$ PES is symmetric with respect to positive and negative torsion angles. Accordingly, the nuclear wavepacket splits into two mirror-symmetric parts during the dynamics. Thus, absolute values of the torsion angle are used in Fig. 3.

Interestingly, an additional degree of freedom was discussed in connection with the induction time in the dynamical simulations of CPD, torsion about the single bond connecting the two double bonds (see ref. 23 and the ESI†). In the case of CPDMe$_6$, its expectation value reaches its new equilibrium value in about 50 fs, the same time as in CPD. In contrast, the induction times of CPD (31 fs) and CPDMe$_6$ (108 fs) differ considerably. Thus, this degree of freedom may not play a substantial role in the induction periods of CPD and CPDMe$_6$.

3.4 Simulated TRPES

1- and 2-photon time-resolved photoelectron spectra of CPDMe$_6$ are simulated using the AIMS trajectory data, with the assumption of the same ionization photon energy as in the TRPES experiments (3.88 eV). In the 1-photon time-resolved photoelectron spectra, only a photoelectron band from ionization of S$_1$ into the lowest cationic state D$_0$ contributes to the spectra. It ranges from 1.4 eV to 0 eV. An additional band of low intensity can be found beyond 1.4 eV. It stems from a single trajectory and, therefore, can be regarded as a statistical artifact due to the limited number of trajectories. In the 2-photon spectra, a photoelectron band from D$_0$ ← S$_1$ transitions is observable between 5.2 eV and 0 eV. Furthermore, a low-energy photoelectron band from ionization into D$_1$ is observable between 2.28 eV and 0 eV.

From 1- and 2-photon spectra, a TRPES spectrum containing both ionization regimes is synthesized (see Fig. 4). Since no

Fig. 4 Simulated time-resolved photoelectron spectra of $CPDMe_6$. Red refers to high, violet to low photoelectron intensities. Two regimes with high (left of yellow line) and low (right of yellow line) photoelectron intensities associated with $[1,1']$ and $[1,2']$ ionization processes respectively can be identified. The intensities in the $[1,2']$ regime are magnified by a factor of 24. The time-delay of the photoelectron bands, the time-zero (t_0) values from a single exponential fit with variable t_0, are inserted as black circles.

absolute 2-photon intensities can be obtained by the employed methods, the electron intensities from the 2-photon spectra were scaled down by a factor of 24, in agreement with the experimental findings. Thus, the contribution from 2-photon signals in regions where 1-photon signals are observed is negligibly small. In analogy with the experimental spectra, this procedure results in a regime with predominant 1-photon photoelectron bands from 0 to 1.8 eV (left of the yellow line in Fig. 4), and a 2-photon regime from 1.8 eV to 5.2 eV (right of yellow line in Fig. 4). The disagreement of the exact energy scales of the 1-photon and 2-photon regimes compared to the experimental observations is attributed to the statistical artifacts in the 1-photon region beyond 1.4 eV, as mentioned above. For improved visualization and, as with the presentation of the experimental data in Fig. 4, the intensities in the 2-photon region were increased to values comparable to the 1-photon region. As in the experimental TRPES, observable features in the 1-photon and the 2-photon regimes are due to the same dynamical processes.

In good agreement with the experimental TRPES, both ionization regimes show a time-delay towards lower photoelectron energies and a simultaneous time-broadening of a single photoelectron band. It is quantified by the same type of fit as in the experimental TRPES. Based on the same argumentation as for the experimental time-resolved photoelectron spectra, the largest delay of (130 ± 1) fs is observed in the 2-photon regime. The intensity modulations observed in the $[1,2']$ regime of the experimental time-resolved photoelectron spectra are not reproduced in the simulation, since multiphoton ionization mechanisms with intermediate resonant Rydberg states were not incorporated into the simulated spectra. There is some discrepancy in the band intensities at very low photoelectron energies due to reduced collection efficiencies for slow electrons caused by field inhomogeneities.

Despite strong similarities of the main observable features, the experimental and simulated TRPES substantially disagree on the overall time scale of the excited state dynamics. For instance, the magnitude of the time-delay differs by more than a factor of two between 310 fs (experimental) and 130 fs (theoretical). As discussed above, this is attributed predominantly to the employed method and approximations in the AIMS simulation.

4 Discussion

4.1 Stepladder-type model for the dynamics

The shifts of the t_0 parameters in the fits of the experimental data as well as the induction time in the fit of the simulated population density evolution are helpful in quantifying the phenomena but not suited to connecting them to common underlying processes. To compare experimental with simulated results and evaluate their qualitative agreement, an analytical model describing the dynamics in S_1 was developed. It describes the wavepacket evolution in the double bond torsion degree of freedom which was identified as governing the dynamics leading from the FC region to the CoIn seam. Moreover, the model reproduces the time evolution of population density, as well as the spectral features arising in the simulated time-resolved photoelectron spectra.

In a simplified approach, the evolution of the wavepacket in the double bond torsion degree of freedom from the FC region to the CoIn seam can be described by a first order rate equation model developed before in ref. 58. Different rate equation models were also used beforehand to describe wavepacket dynamics in the excited state.[5,59,60] Using first order kinetics, the evolution of the wavepacket in the double bond torsion degree of freedom from the FC region to the CoIn seam can be described by time-dependent statistical distribution over a "stepladder" consisting of a number of discrete steps connected by an uniform transfer time constant τ_s, as schematically depicted in Fig. 5. Each step has a slightly different ionization potential and, therefore, a different

Fig. 5 Visualization of the proposed stepladder-type model for the vibrational redistribution dynamics in S_1. Population evolution takes place via a step by step process, whereas the probability for transition to the next lower step is characterized by the uniform time constant τ_s. As indicated by the dark blue arrows, each step has a slightly different spectral signature. Population which has returned to the ground state (S_0) is not detected due to insufficient Franck–Condon overlap.
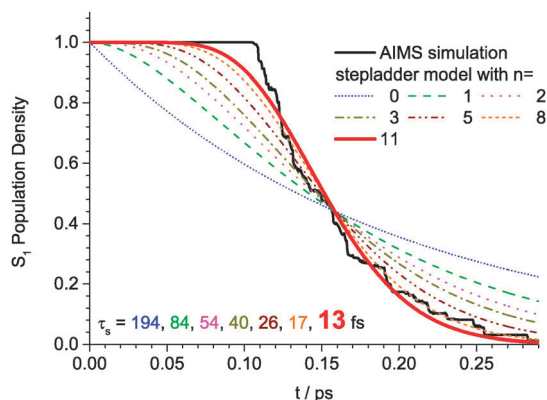
Fig. 6 Fit of the simulated S_1 population density evolution by functions of the type given by eqn (2), employing different values of n. The corresponding values of τ_s are additionally listed. The best fit is obtained with $n = 11$ (red curve) and yields a time-step of $\tau_s = 13$ fs.

spectral signature (photoelectron kinetic energy). Details of the model are elaborated in ref. 58 and in the ESI.† They lead to the following expression for the time evolution of population density $P_{S_1}(t)$

$$P_{S_1}(t) = e^{-\frac{t}{\tau_s}} \sum_{j=0}^{n} \frac{t^j}{j! \tau_s^j}, \tag{2}$$

where n corresponds to the number of steps in S_1.

Eqn (2) can be compared to the population density evolution from the $CPDMe_6$ dynamics simulations. Two parameters must be optimized, n and τ_s. As can be seen in Fig. 6, except for a single-step model, all other numbers of steps yield functions exhibiting an induction period without loss of population density and a delayed S-type decay. Different numbers of steps yield quite different fit qualities and the optimized values of τ_s are highly dependent on the number of steps. The best fit (χ^2 value) can be obtained with 12 steps (corresponding to $n = 11$ in eqn (2)). The optimized value of τ_s is in this case (13 ± 1) fs. Since the number of steps and the value of τ_s are highly convoluted, they cannot directly serve as parameters with any physical meaning. However, a characteristic time parameter for the population evolution (t_{ch}) can be obtained by evaluating the point of inflection of the S-shaped decay (see the ESI†),

$$t_{ch} = n \cdot \tau_s = (140 \pm 10) \text{ fs}. \tag{3}$$

Model and simulated population density evolution agree well except for the section where population density loss begins. This deviation might not only be attributed to the deficiencies of the model. Due to the statistics being limited by the number of trajectories, the tails of the wavepacket cannot be represented sufficiently well by the dynamical simulation. Since the onset of population density loss coincides with the arrival of the leading tail of the wavepacket at the CoIn seam, especially in this region the occurrence of statistical artifacts can be expected. A considerable increase in the number of trajectories would most probably smooth out the onset of population loss.

In order to determine if the simple stepladder model can also reproduce the energy shift of the photoelectron bands in the simulated time-resolved photoelectron spectra, each step can be correlated with a spectral signature $A_j(E_{kin})$. The band shift was observed in both simulated and experimental time-resolved photoelectron spectra from higher to lower photoelectron energies. The vertical IPs and therefore the signatures of the steps are also expected to be shifted to lower photoelectron kinetic energies, due to large amplitude motions between FC region and CoIn seam (see Fig. 5). Including the instrument response function $g(\tau)$ results in a fit function $S(E_{kin}, \tau)$ for the spectra:

$$S(E_{kin}, \tau) = g(\tau) \otimes e^{-\frac{\tau}{\tau_s}} \sum_{j=0}^{n} \frac{A_j(E_{kin}) \tau^j}{j! \tau_s^j} \tag{4}$$

For the fitting procedure, the simulated spectra were cut into slices of $\Delta E = 0.1$ eV. The spectra can be fitted with satisfactory accuracy with fixed values $n = 11$ and $\tau_s = 13$ fs, as derived from the population density fit. The amplitude spectra (see the ESI†) indeed show the expected shift to lower photoelectron energies.

An analogous fit was also applied to the experimental time-resolved photoelectron spectra. As before, n is thereby set to 11. The details of the fit and the amplitude spectra are given in the ESI.† For t_{ch} a value of (540 ± 30) fs was obtained. This value is considerably larger than the spectral shift of (310 ± 20) fs quantified *via* an exponential fit with varying time zero parameters. However, it has to be kept in mind that t_{ch} is a single parameter quantifying the overall excited state dynamics, whereas the range of time zero parameters is solely a measure for the spectral shift and is only capable of modelling the time-resolved photoelectron spectra in connection with an additional parameter, an exponential time constant.

As in the amplitude spectra of the simulated data, a shift of the spectra towards lower photoelectron energies is clearly observable. Thus, the qualitative results from evaluation of the AIMS simulations nicely agree with evaluation of the experimental data.

Hence, *via* use of this simple stepladder model, the observation of the photoelectron band shift can be directly attributed to wavepacket evolution in a distinct vibrational degree of freedom, torsion about one of the double bonds. Moreover, by introducing the single model parameter t_{ch}, the theoretical as well as the experimental observations of the excited state dynamics of $CPDMe_6$ including the two phenomena induction time and photoelectron spectral shift are satisfactorily described and quantified. Reduction of the excited state dynamics to a one-dimensional relaxation coordinate provides a very intuitive picture for understanding the connection between the process and how it is observed in TRPES. However, it may be too simplified for describing other aspects of multi-dimensional excited state dynamics (see *e.g.* ref. 19, 23 and 61).

4.2 Generalization to other polyenes

Our experimental and theoretical findings on $CPDMe_6$ presented above agree well with each other and are in line with

AIMS simulations of CPD. Although the TRPES data for CPD and its derivatives were earlier analyzed *via* a biexponential fit,[9,10] we here show on the example of CPDMe$_4$PrH that the dynamics can be described equally well *via* a single exponential decay and a shift in time zero or a fit according to eqn (4). The most appropriate model can only be chosen with the help of the theoretical knowledge of the underlying dynamics and the direct simulations of observables.

Associating the photoelectron band shift of CPDMe$_6$ with one double bond torsion coordinate connects it with localization of the dynamics at one of the ethylene units of CPDMe$_6$, leaving the other ethylene as a "spectator"-unit relatively unaltered. This observation is strongly in line with the concept of dynamophore subunits governing and localizing ultrafast dynamics in cyclic polyenes, as described in ref. 12 and 33. Similar but weaker photoelectron band shifts were indeed observed earlier in cyclic polyenes like cyclohexa-1,4-diene (100 fs), cyclohexene (90 fs) and cycloheptatriene (30 fs)[12,17] and also in considerably larger polyenic systems.[11] They were associated to large amplitude motions of the nuclear wave-packet and localization of the dynamics on the way to the CoIn with the ground state. However, a quantitative assignment to particular degrees of freedom was not possible due to the lack of detailed dynamics simulations of these molecules.

The situation is different for the smallest non-cyclic unsaturated hydrocarbons ethylene and butadiene. In ethylene, an induction period prior to exponential ground state recovery of about 40 fs was observed in several theoretical studies and is mostly associated with a twist around the double bond.[22,25,26] Furthermore, simulated time-resolved photoelectron spectra show band shifts on a similar time scale.[25,29] Experimentally resolving and quantifying a delay of 40 fs in a photoelectron band is still a huge challenge. However, hints for such a shift can also be found in published TRPES data of ethylene, although analyzed differently there.[13]

In butadiene, an induction period of about 50 fs was observed in simulations.[21] In this case, it can be connected to two vibrational degrees of freedom, the dihedral angle between the two conjugated double bonds and a double bond torsion angle. Furthermore, experimental time-resolved photoelectron–photoion coincidence spectra of butadiene clearly resolve a shift by 20 fs and a broadening by 30 fs of the photoelectron band at time zero, which seems comparable to our observations in CPDMe$_6$.[16,33]

Our observations of excited state dynamics in CPDMe$_6$ seem to be of more general validity for small polyenes. However, this clearly has to be checked thoroughly with different model systems by further combinations of experimental and theoretical investigations.

5 Conclusions

CPDMe$_6$ serves as an excellent benchmark molecule with which observations made in TRPES and AIMS dynamics simulations can be connected. It exhibits a large spectral shift during a (310 ± 20) fs period in the experimental time-resolved photoelectron spectra and shows a substantial induction period of (108 ± 1) fs in the simulated dynamics. The discrepancy between the time scales can be attributed to the approximation of methyl substituents as hydrogens with mass 15 in the AIMS simulations. The induction period can be associated with a distinct vibrational degree of freedom, namely torsion about one of the double bonds. This molecule therefore constitutes another example of dynamics with an ethylenic dynamophore. A simple stepladder-type model is developed giving a one-dimensional and therefore very intuitive approach to the dynamics by reducing their description to a single localized degree of freedom. The simple stepladder model fits the overall population density evolution as well as experimental and simulated TRPES data with only one characteristic time parameter t_{ch} of (140 ± 10) fs (simulation) and (540 ± 30) fs (experiment). Hence, it can directly connect localization of the dynamics, the induction time and the shift in the time-resolved photoelectron spectra in CPDMe$_6$. The combination of TRPES and AIMS simulations is shown to be especially suited to connecting experimental observables to underlying dynamical processes. Comparison to other small polyenes suggests that the validity of this connection is not restricted to CPDMe$_6$ but may more generally apply to polyenic systems.

References

1 P. Farmanara, V. Stert and W. Radloff, *Chem. Phys. Lett.*, 1998, **288**, 518–522.

2 F. Assenmacher, M. Gutmann, G. Hohlneicher, V. Stert and W. Radloff, *Phys. Chem. Chem. Phys.*, 2001, **3**, 2981–2982.

3 S. Lochbrunner, T. Schultz, M. Schmitt, J. P. Shaffer, M. Z. Zgierski and A. Stolow, *J. Chem. Phys.*, 2001, **114**, 2519–2522.

4 V. Stert, H. Lippert, H.-H. Ritze and W. Radloff, *Chem. Phys. Lett.*, 2004, **388**, 144–149.

5 W. Fuß, W. E. Schmid and S. Trushin, *Chem. Phys.*, 2005, **316**, 225–234.

6 A. M. D. Lee, J. D. Coe, S. Ullrich, M.-L. Ho, S.-J. Lee, B.-M. Cheng, M. Z. Zgierski, I.-C. Chen, T. J. Martínez and A. Stolow, *J. Phys. Chem. A*, 2007, **111**, 11948–11960.

This journal is © the Owner Societies 2014

Phys. Chem. Chem. Phys., 2014, **16**, 11770–11779 | 11777

7 K. Kosma, S. A. Trushin, W. Fuss and W. E. Schmid, *J. Phys. Chem. A*, 2008, **112**, 7514–7529.

8 F. Rudakov and P. M. Weber, *Chem. Phys. Lett.*, 2009, **470**, 187–190.

9 F. Rudakov and P. M. Weber, *J. Phys. Chem. A*, 2010, **114**, 4501–4506.

10 O. Schalk, A. E. Boguslavskiy and A. Stolow, *J. Phys. Chem. A*, 2010, **114**, 4058–4064.

11 R. Y. Brogaard, A. E. Boguslavskiy, O. Schalk, G. D. Enright, H. Hopf, V. A. Raev, P. G. Jones, D. L. Thomsen, T. I. Sølling and A. Stolow, *Chem. – Eur. J.*, 2011, **17**, 3922–3931.

12 O. Schalk, A. E. Boguslavskiy, A. Stolow and M. S. Schuurman, *J. Am. Chem. Soc.*, 2011, **133**, 16451–16458.

13 G. Wu, A. E. Boguslavskiy, O. Schalk, M. S. Schuurman and A. Stolow, *J. Chem. Phys.*, 2011, **135**, 164309.

14 A. E. Boguslavskiy, M. S. Schuurman, D. Townsend and A. Stolow, *Faraday Discuss.*, 2011, **150**, 419–438.

15 V. S. Petrović, M. Siano, J. L. White, N. Berrah, C. Bostedt, J. D. Bozek, D. Broege, M. Chalfin, R. N. Coffee, J. Cryan, L. Fang, J. P. Farrell, L. J. Frasinski, J. M. Glownia, M. Gühr, M. Hoener, D. M. P. Holland, J. Kim, J. P. Marangos, T. Martínez, B. K. McFarland, R. S. Minns, S. Miyabe, S. Schorb, R. J. Sension, L. S. Spector, R. Squibb, H. Tao, J. G. Underwood and P. H. Bucksbaum, *Phys. Rev. Lett.*, 2012, **108**, 253006.

16 P. Hockett, E. Ripani, A. Rytwinski and A. Stolow, *J. Mod. Opt.*, 2013, **60**, 1409–1425.

17 O. Schalk, A. E. Boguslavskiy, M. S. Schuurman, R. Y. Brogaard, A.-N. Unterreiner, A. Wrona-Piotrowicz, N. H. Werstiuk and A. Stolow, *J. Phys. Chem. A*, 2013, **117**, 10239–10247.

18 T. I. Sølling, T. S. Kuhlman, A. B. Stephansen, L. B. Klein and K. B. Møller, *ChemPhysChem*, 2014, **15**, 249–259.

19 L. Poisson, D. Nandi, B. Soep, M. Hochlaf, M. Boggio-Pasqua and J.-M. Mestdagh, *Phys. Chem. Chem. Phys.*, 2014, **16**, 581–587.

20 M. Ben-Nun, J. Quenneville and T. J. Martínez, *J. Phys. Chem. A*, 2000, **104**, 5161–5175.

21 B. G. Levine and T. J. Martínez, *J. Phys. Chem. A*, 2009, **113**, 12815–12824.

22 H. Tao, B. G. Levine and T. J. Martínez, *J. Phys. Chem. A*, 2009, **113**, 13656–13662.

23 T. S. Kuhlman, W. J. Glover, T. Mori, K. B. Møller and T. Martínez, *Faraday Discuss.*, 2012, **157**, 193–212.

24 A. L. Thompson and T. J. Martínez, *Faraday Discuss.*, 2011, **150**, 293–311.

25 T. Mori, W. J. Glover, M. S. Schuurman and T. J. Martínez, *J. Phys. Chem. A*, 2012, **116**, 2808–2818.

26 B. Sellner, M. Barbatti, T. Müller, W. Domcke and H. Lischka, *Mol. Phys.*, 2013, **111**, 2439–2450.

27 H. R. Hudock, B. G. Levine, A. L. Thompson, H. Satzger, D. Townsend, N. Gador, S. Ullrich, A. Stolow and T. J. Martínez, *J. Phys. Chem. A*, 2007, **111**, 8500–8508.

28 T. Fuji, Y.-I. Suzuki, T. Horio, T. Suzuki, R. Mitrić, U. Werner and V. Bonačić-Koutecký, *J. Chem. Phys.*, 2010, **133**, 234303.

29 H. Tao, T. K. Allison, T. W. Wright, A. M. Stooke, C. Khurmi, J. van Tilborg, Y. Liu, R. W. Falcone, A. Belkacem and T. J. Martínez, *J. Chem. Phys.*, 2011, **134**, 244306.

30 R. Y. Brogaard, T. I. Sølling and K. B. Møller, *J. Phys. Chem. A*, 2011, **115**, 556–561.

31 T. K. Allison, H. Tao, W. J. Glover, T. W. Wright, A. M. Stooke, C. Khurmi, J. van Tilborg, Y. Liu, R. W. Falcone, T. J. Martínez and A. Belkacem, *J. Chem. Phys.*, 2012, **136**, 124317.

32 G. Wu, P. Hockett and A. Stolow, *Phys. Chem. Chem. Phys.*, 2011, **13**, 18447–18467.

33 O. Schalk, A. E. Boguslavskiy, M. S. Schuurman and A. Stolow, *EPJ Web Conf.*, 2013, **41**, 2037.

34 K. B. Møller and A. H. Zewail, *Chem. Phys. Lett.*, 1998, **295**, 1–10.

35 K. B. Møller, N. E. Henriksen and A. H. Zewail, *J. Chem. Phys.*, 2000, **113**, 10477–10485.

36 V. Blanchet, M. Z. Zgierski, T. Seideman and A. Stolow, *Nature*, 1999, **401**, 52–54.

37 H. Hippler, M. Olzmann, O. Schalk and A.-N. Unterreiner, *Z. Phys. Chem.*, 2005, **219**, 389–398.

38 N. Christensson, T. Polivka, A. Yartsev and T. Pullerits, *Phys. Rev. B: Condens. Matter Mater. Phys.*, 2009, **79**, 245118.

39 T. Kovar and H. Lischka, *J. Mol. Struct.*, 1994, **303**, 71–82.

40 M. Ben-Nun and T. J. Martínez, *Adv. Chem. Phys.*, 2002, **121**, 439–512.

41 S.-H. Lee, K.-C. Tang, I.-C. Chen, M. Schmitt, J. P. Shaffer, T. Schultz, J. G. Underwood, M. Z. Zgierski and A. Stolow, *J. Phys. Chem. A*, 2002, **106**, 8979–8991.

42 S. Lochbrunner, J. J. Larsen, J. P. Shaffer, M. Schmitt, T. Schultz, J. G. Underwood and A. Stolow, *J. Electron Spectrosc. Relat. Phenom.*, 2000, **112**, 183–198.

43 G. K. Jarvis, M. Evans, C. Y. Ng and K. Mitsuke, *J. Chem. Phys.*, 1999, **111**, 3058–3069.

44 H.-J. Werner, *Mol. Phys.*, 1996, **89**, 645–661.

45 J. Finley, P.-A. Malmqvist, B. O. Roos and L. Serrano-Andrés, *Chem. Phys. Lett.*, 1998, **288**, 299–306.

46 T. Shiozaki, W. Győrffy, P. Celani and H.-J. Werner, *J. Chem. Phys.*, 2011, **135**, 081106.

47 H.-J. Werner, P. J. Knowles, R. Lindh, F. R. Manby, M. Schütz, P. Celani, T. Korona, G. Rauhut, R. D. Amos, A. Bernhardsson, A. Berning, D. L. Cooper, M. J. O. Deegan, A. J. Dobbyn, F. Eckert, C. Hampel, G. Hetzer, A. Lloyd, S. J. McNicholas, W. Meyer, M. E. Mura, A. Nicklass, P. Palmieri, R. Pitzer, U. Schumann, H. Stoll, A. J. Stone, R. Tarroni and T. Thorsteinsson, *MOLPRO, version 2006.1, a package of ab initio programs*, see: http://www.molpro.net.

48 B. G. Levine, J. D. Coe and T. J. Martínez, *J. Phys. Chem. B*, 2008, **112**, 405–413.

49 B. G. Levine, J. D. Coe, A. M. Virshup and T. J. Martínez, *Chem. Phys.*, 2008, **347**, 3–16.

50 T. Mori and S. Kato, *Chem. Phys. Lett.*, 2009, **476**, 97–100.

51 M. D. Hack, A. M. Wensmann, D. G. Truhlar, M. Ben-Nun and T. J. Martínez, *J. Chem. Phys.*, 2001, **115**, 1172–1186.

52 L. Tao, C. Oana, V. Mozhayskiy and A. Krylov, *ezDyson*, http://iopenshell.usc.edu/downloads/ezdyson.

53 M. J. Frisch, G. W. Trucks, H. B. Schlegel, G. E. Scuseria, M. A. Robb, J. R. Cheeseman, G. Scalmani, V. Barone, B. Mennucci, G. A. Petersson, H. Nakatsuji, M. Caricato, X. Li, H. P. Hratchian, A. F. Izmaylov, J. Bloino, G. Zheng, J. L. Sonnenberg, M. Hada, M. Ehara, K. Toyota, R. Fukuda, J. Hasegawa, M. Ishida, T. Nakajima, Y. Honda, O. Kitao, H. Nakai, T. Vreven, J. A. Montgomery, Jr., J. E. Peralta, F. Ogliaro, M. Bearpark, J. J. Heyd, E. Brothers, K. N. Kudin, V. N. Staroverov, R. Kobayashi, J. Normand, K. Raghavachari, A. Rendell, J. C. Burant, S. S. Iyengar, J. Tomasi, M. Cossi, N. Rega, J. M. Millam, M. Klene, J. E. Knox, J. B. Cross, V. Bakken, C. Adamo, J. Jaramillo, R. Gomperts, R. E. Stratmann, O. Yazyev, A. J. Austin, R. Cammi, C. Pomelli, J. W. Ochterski, R. L. Martin, K. Morokuma, V. G. Zakrzewski, G. A. Voth, P. Salvador, J. J. Dannenberg, S. Dapprich, A. D. Daniels, Ö. Farkas, J. B. Foresman, J. V. Ortiz, J. Cioslowski and D. J. Fox, *Gaussian 09 Revision A.02*, Gaussian Inc., Wallingford, CT, 2009.

54 F. Weigend, F. Furche and R. Ahlrichs, *J. Chem. Phys.*, 2003, **119**, 12753–12762.

55 O. Schalk, M. S. Schuurman, G. Wu, P. Lang, M. Mucke, R. Feifel and A. Stolow, *J. Phys. Chem. A*, 2014, **118**, 2279–2287.

56 A. Stolow and J. G. Underwood, *Advances in Chemical Physics*, Wiley, 2008, vol. 139, p. 497.

57 P. Hockett, C. Z. Bisgaard, O. J. Clarkin and A. Stolow, *Nat. Phys.*, 2011, **7**, 612–615.

58 K. B. Møller and A. H. Zewail, *Chem. Phys. Lett.*, 2002, **351**, 281.

59 S. A. Trushin, W. Fuss, K. L. Kompa and W. E. Schmid, *J. Phys. Chem. A*, 2000, **104**, 1997–2006.

60 W. Fuß, W. E. Schmid and S. A. Trushin, *J. Chem. Phys.*, 2000, **112**, 8347–8362.

61 W. Fuß, *Chem. Phys.*, 2013, **425**, 96.

This journal is © the Owner Societies 2014

Phys. Chem. Chem. Phys., 2014, **16**, 11770–11779 | 11779